CELLULAR NEUROSCIENCE

Novel self-replicating α-synuclein polymorphs that escape ThT monitoring can spontaneously emerge and acutely spread in neurons

Francesca De Giorgi[1,2,3]*, Florent Laferrière[1,2]*, Federica Zinghirino[1,2,4], Emilie Faggiani[1,2], Alons Lends[5], Mathilde Bertoni[5], Xuan Yu[6], Axelle Grélard[5], Estelle Morvan[7], Birgit Habenstein[5], Nathalie Dutheil[1,2], Evelyne Doudnikoff[1,2], Jonathan Daniel[8], Stéphane Claverol[9], Chuan Qin[6], Antoine Loquet[5], Erwan Bezard[1,2], François Ichas[1,2,3]†

The conformational strain diversity characterizing α-synuclein (α-syn) amyloid fibrils is thought to determine the different clinical presentations of neurodegenerative diseases underpinned by a synucleinopathy. Experimentally, various α-syn fibril polymorphs have been obtained from distinct fibrillization conditions by altering the medium constituents and were selected by amyloid monitoring using the probe thioflavin T (ThT). We report that, concurrent with classical ThT-positive products, fibrillization in saline also gives rise to polymorphs invisible to ThT (τ^-). The generation of τ^- fibril polymorphs is stochastic and can skew the apparent fibrillization kinetics revealed by ThT. Their emergence has thus been ignored so far or mistaken for fibrillization inhibitions/failures. They present a yet undescribed atomic organization and show an exacerbated propensity toward self-replication in cortical neurons, and in living mice, their injection into the substantia nigra pars compacta triggers a synucleinopathy that spreads toward the dorsal striatum, the nucleus accumbens, and the insular cortex.

INTRODUCTION

α-Synuclein (α-syn) is a small ubiquitous protein that is especially abundant in the brain. In neurons, α-syn is presynaptically enriched and associates with the neurosecretory vesicles as α-helical multimers (*1*), while its C terminus interacts with vesicle-associated membrane protein 2 (VAMP2) (*2*). Under this conformation, α-syn regulates the kinetics of neurotransmitter release in the synaptic cleft (*1*, *2*). Before becoming associated with the membrane of presynaptic vesicles, however, α-syn transits in the neuronal cytosol as its free, soluble, monomeric form (*1*, *3*, *4*). In this latter context, α-syn oscillates between a variety of different conformational states: It is an intrinsically disordered protein (*5*). Certain conformations that are enriched in beta folds can incidentally get favored and stabilized (*6*). Their nucleation forms "seeds" that trigger the templated growth of amyloid structures building up at the expense of neuronal α-syn. This process results in the formation of long intraneuronal amyloid fibrils that partly get packed and stored in inclusion bodies called Lewy bodies (LBs) (*7*) and partly get passed to neighboring neurons where they propagate the amyloid build-up process (*8*, *9*). This self-regenerative mechanism provides an explanation for the progressive intracerebral spread of LBs observed during Parkinson's disease (PD) progression (*10*) and for the gradual worsening of other synucleinopathies (*11*).

Notably, during amyloid stacking, α-syn can adopt several distinct structural folds, resulting in the emergence of fibril polymorphs (*12*–*18*). Together with their specific fold, their supramolecular properties also get inherited and propagated as the polymorphs self-replicate by templated growth (*19*–*22*). It is thus tempting to speculate that the distinctive properties of these different polymorphs are responsible for the different clinical presentation of the neurodegenerative diseases that are underpinned by a synucleinopathy (*23*–*25*). We noticed, however, that the biological characterization of structurally defined α-syn polymorphs had often been limited to the demonstration of their cellular "toxicity" or "pro-aggregative" action without consideration of their ability to reproduce their distinctive amyloid fold inside cells. The original aim of our study was, thus, to determine whether structurally characterized α-syn polymorphs could demonstrate autonomous self-replication of their structural traits during propagation not only in vitro but also in living neurons. We incidentally found the existence of τ^- amyloid polymorphs acutely spreading in neurons. Not only were these τ^- amyloids invisible to thioflavin T (ThT), but also they could be preferentially revealed using SYBR Green. On the basis of this, we designed a simple multiplexed assay (which we termed the "fibrilloscope") to track their propensity toward self-replication.

[1]CNRS, Institut des Maladies Neurodégénératives, UMR 5293, Bordeaux, France. [2]Université de Bordeaux, Institut des Maladies Neurodégénératives, UMR 5293, Bordeaux, France. [3]INSERM, Laboratoire de Neurosciences Expérimentales et Cliniques, U-1084, Université de Poitiers, Poitiers, France. [4]Dipartimento di Scienze Biomediche e Biotecnologiche (BIOMETEC), Università degli Studi di Catania, Catania, Italia. [5]Institut de Chimie et de Biologie des Membranes et des Nano-objets, Institut Européen de Chimie et Biologie, CNRS, UMR 5248, Université de Bordeaux, Pessac, France. [6]Institute of Laboratory Animal Sciences, China Academy of Medical Sciences, Beijing, China. [7]Université de Bordeaux, CNRS, INSERM, UMS3033/US001, Institut Européen de Chimie et Biologie, Pessac, France. [8]Institut des Sciences Moléculaires, CNRS, UMR 5255, Université de Bordeaux, Talence, France. [9]Plateforme de Protéomique, Université de Bordeaux, Bordeaux, France.
*These authors contributed equally to this work.
†Corresponding author. Email: francois.ichas@inserm.fr

RESULTS

τ^- α-syn assemblies emerge and cause neuronal synucleinopathy

We first sought (i) to isolate/characterize different α-syn polymorphs self-assembled under simple shaking in saline (see Materials and Methods) and (ii) to determine whether these "untouched" assemblies could self-replicate and spread in neurons (untouched meaning here "without artificially disrupting the assemblies using sonication"). A single batch of "NMR (nuclear magnetic resonance)–grade" recombinant α-syn (labeled with ^{13}C and ^{15}N) was divided into seven identical aliquots (Fig. 1A). One was left at 4°C; the other six were

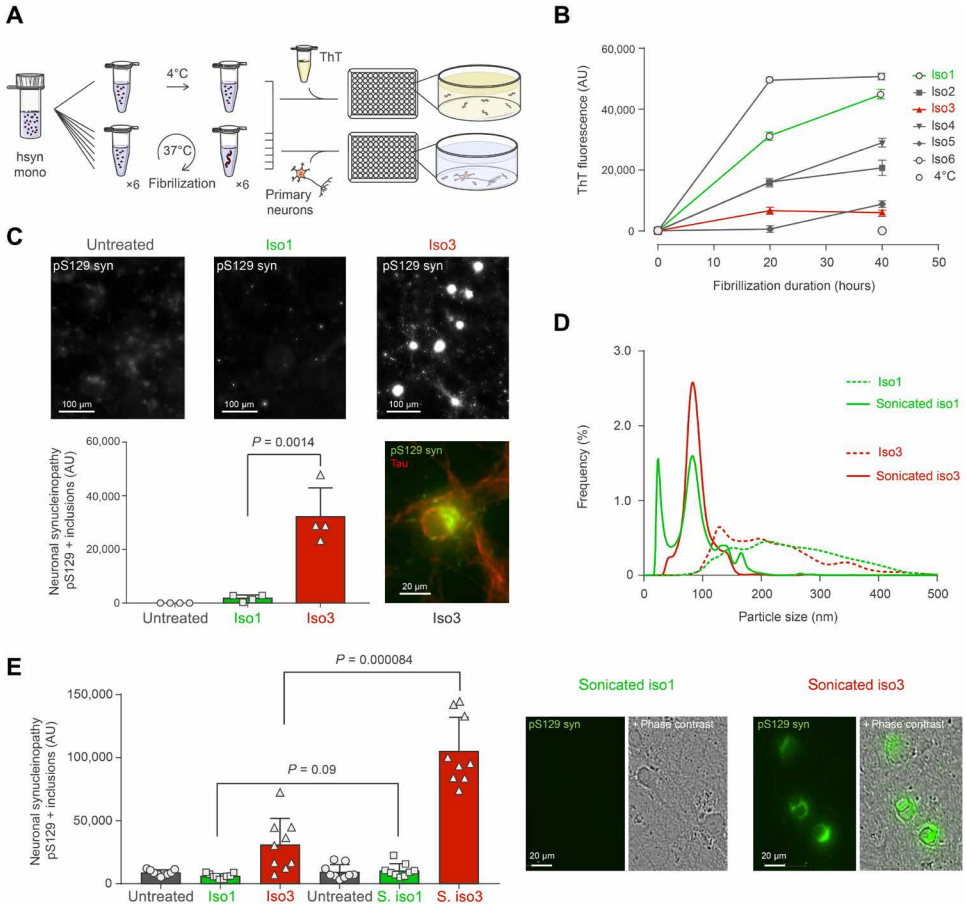

Fig. 1. Spontaneous emergence of α-syn assemblies that escape amyloid monitoring by ThT and show exacerbated spread in neurons. (**A**) Schematic representation of the fibrillization and testing workflow. (**B**) Development of the ThT signal in the six α-syn tubes, sampled after 0, 20, and 40 hours of shaking at 37°C or for 40 hours for the unshaken, 4°C tube. Three measurement replicates for each sample and time point. (**C**) HCA of the synucleinopathy induced by 10 nM (equivalent monomeric α-syn concentration) of untouched iso1 and iso3 in primary mouse cortical neurons ($n = 4$, nine measures per replicate, intrareplicate measurement means are shown). Quantitation and representative imaging fields are shown with a full intensity range lookup table (visual saturation of the highest pixel values). Scale bars, 100 μm. Close-up of the iso3 condition with an intensity range lookup table focused on the highest pixel values, showing pS129 syn in green and tau in red. The somatic pS129 syn aggregates are perikaryal. (**D**) NTA shows that untouched iso1 is not more clumped than iso3 and that sonication decreases the size of the assemblies present in both samples. Note that iso1 is more frangible than iso3 with a distinctive size peak at 25 to 50 nm appearing after sonication for iso1. The spectra shown correspond to the average of five consecutive detection runs per sample. (**E**) The lack of neuronal activity of iso1 in the HCA assay is not enhanced by sonication, while the one of iso3 is increased ($n = 3$, nine measurement fields per replicate; data points: interreplicate mean of randomly matched fields). Corresponding representative HCA close-ups showing pS129 and phase contrast for sonicated iso1 and iso3. *P* values of the group differences were calculated using *t* test. AU, arbitrary units.

then shaken together. Notably, using the classical amyloid probe ThT (*26*) to monitor the fibrillization (*17*, *18*, *27*), we observed a major variability in the development of the ThT signal from one tube to another (Fig. 1B). Certain aliquots showed a very rapid and strong rise in ThT fluorescence; others had a slower increase but reaching comparable final values, and others had an almost flat ThT curve. As it is widely assumed that the buildup of a ThT signal under these conditions is synonymous with proper α-syn amyloid assembly (*17*, *18*) [see current best practice guidelines (*27*)], we simply sought to compare the bioactivity of iso1, a presumably "successfully fibrillized" ThT-high sample, with that of iso3, a presumably "failed" ThT-low sample. To that end, we developed and validated a high-content analysis (HCA) assay based on primary mouse cortical neurons (*28*, *29*), allowing the observation of a seeded synucleinopathic buildup in fully mature primary cultures (30 days in vitro) (fig. S1) [see also (*30*)]. The neurons were challenged with iso1 and iso3, immediately upon completion of the 40-hour fibrillization period without any other manipulation (untouched). The results (Fig. 1C) were completely opposite to expectation: Iso3, which according to ThT was supposed to be virtually devoid of amyloids (*27*), induced a massive synucleinopathy, causing a widespread buildup of secondary aggregates, while no synucleinopathy developed in the neurons treated with the ThT-positive iso1. To explain this counterintuitive lack of activity, we reasoned that unspecific clumping could have incidentally occurred in the iso1 sample, impeding neuronal uptake of the seeds. However, using nanoparticle tracking analysis (NTA), no clumping was detectable in iso1 compared to iso3 (Fig. 1D, dotted lines). Nevertheless, we proceeded with sonication that drastically reduced the size of the particles in both samples, producing a distinctive peak of smaller 25- to 50-nm-wide particles in iso1 that was absent in sonicated iso3 (Fig. 1D, solid lines). With particle size reduction, sonicated iso3 exhibited an increased activity in neurons

(Fig. 1E). Sonicated iso1 was, however, still unable to trigger a synucleinopathy (Fig. 1E).

τ⁻ α-syn polymorphism

We thus proceeded with a further comparative characterization of iso1 and iso3 using the Congo red derivative X-34 (Fig. 2A) (*31*), density floatation (Fig. 2B), velocity sedimentation (Fig. 2C) (*32*), and electron microscopy (Fig. 2D). All these approaches indicated that iso3 contained as much α-syn amyloid assemblies as iso1, with the iso3 fibrils appearing slightly shorter but straighter and more often bundled at an ultrastructural level (Fig. 2D). Although this became apparent only after sonication using NTA, velocity sedimentation by ultracentrifugation in the presence of sarkosyl revealed that the native amyloid assemblies populating iso1 and iso3 had different size distribution patterns. Iso1 contained smaller assemblies than iso3 (Fig. 2C). However, the similarity of the density floatation patterns observed for iso1 and iso3 (Fig. 2B) indicated that all the amyloid assemblies present in the two preparations shared a common and unique amyloid compactness, irrespective of their size. Overall, these data pointed to the possibility that iso1 and iso3 contained two distinct amyloid α-syn polymorphs that had spontaneously emerged from a single condition and endowed with (i) distinct "all-or-none" ThT visibilities and (ii) distinct all-or-none natural propensities to spread in mouse neurons. This possibility was strengthened by the observation that 23 days after treatment, higher levels of iso3 persisted inside neurons compared to iso1 (Fig. 2E), a result compatible with the notion that distinct α-syn polymorphs could be cleared with different efficiencies in neurons (*33*).

We thus performed two-dimensional (2D) solid-state NMR spectroscopy to assess the hNH (Fig. 2F) and hCH (fig. S2A) spectral fingerprints of the fully protonated iso1 and iso3 samples at fast magic angle spinning (100 kHz). Iso1 and iso3 exhibited two clearly distinct structural conformations at the atomic level, as revealed by two different single sets of chemical shift resonances. Both NMR fingerprints exhibited a single set of sharp signals, indicating the presence in each sample of a single nonpolymorphic amyloid structure, highly ordered at the atomic level.

Furthermore, we recorded 3D hCANH experiments on iso1 and iso3 to extract 2D NCA planes and compared them to previous solid-state NMR data of four different polymorphs (*13*–*16*) spanning the entire structure family spectrum defined by Guerrero-Ferreira and co-workers (*18*) (fig. S2B).

Notably, iso1 turned out to correspond to the "type 2" fibril polymorph species (fig. S2B) (*14*, *18*). As to the stealth polymorph iso3, there was no match with any of the polymorph structure families previously characterized (fig. S2B) (*13*–*18*). However, despite their structural differences (documented in the panel iso3 versus "Gath *et al.* 2011 tris 5 mM" in fig. S2B), iso3 shares its "ThT invisibility" with the "ribbon" amyloids assembled under low-salt conditions (*13*, *19*). A feature of ribbons that stands out compared to all other fibril types is the particular beta structure of the N terminus (*16*): This could suggest the possible existence of a similar trait in iso3. These results indicate that α-syn can spontaneously and randomly assemble into distinct amyloids under a single experimental condition and that previously unnoticed ThT-negative polymorphs (τ⁻ polymorphs) can proliferate, crowd the fibrillar population, and cause exacerbated neuronal spread.

Note that the spontaneous emergence of distinct polymorphs seen here could either reflect a stochastic process taking place

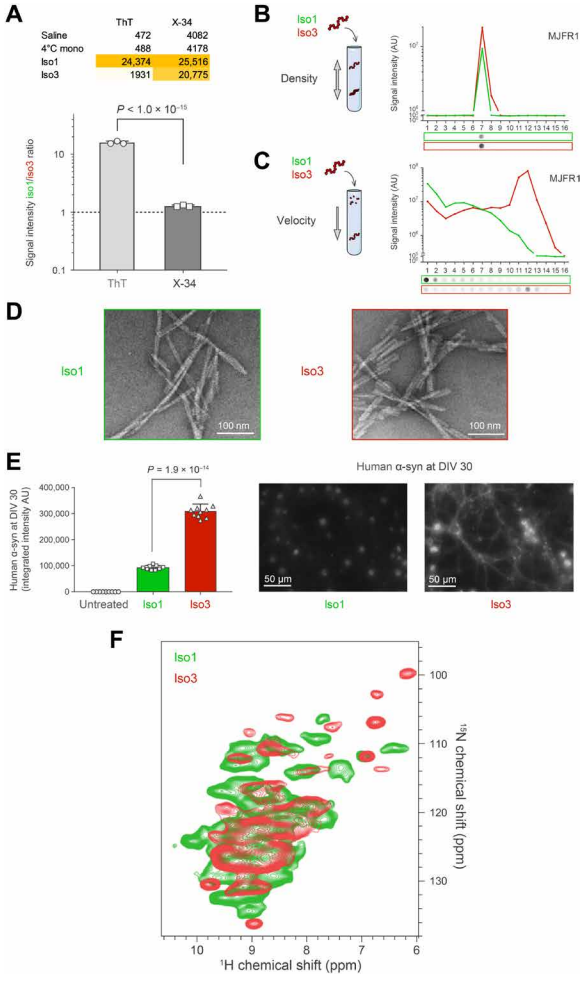

Fig. 2. Iso3 is a novel ThT-invisible (τ⁻) fibrillary polymorph. (**A**) Fluorescence of the amyloid probe X-34 indicates that there are same amounts of amyloids in iso1 and iso3 despite an over 10-fold difference in ThT signal; table with mean values ($n = 3$) and corresponding graph with iso1 to iso3 signal ratios. *P* values of the group differences were calculated using *t* test. (**B**) Schematic representation of the density floatation protocol: Iso1 and iso3 were solubilized with sarkosyl, loaded in the middle of iodixanol gradients, and fractionated by density upon isopycnic equilibrium ultracentrifugation. The collected fractions (numbered from top to bottom of the gradient) were analyzed for human α-syn content (using the anti-human α-syn antibody MJFR1) by filter trap (representative pictures of the immunoblots under the graph) by quantification from $n = 3$ replicates of the absolute chemiluminescence signal (AU, graph). Data presented are the mean curves for each group. (**C**) Schematic representation of the sedimentation velocity protocol: Iso1 and iso3 were solubilized with sarkosyl and loaded on top of linear iodixanol gradients and fractionated by sedimentation velocity upon ultracentrifugation. The collected fractions were collected and revealed/quantified as in (B). While the density of the iso1 and iso3 amyloid assemblies are strictly equal and monodisperse (B), their size distributions are different (C). (**D**) Transmission electron micrographs of iso1 and iso3 showing their prototypical fibrillary structure. (**E**) Neuronal persistence of iso1 and iso3 at DIV 30 (23 days after treatment) imaged and quantified by HCA using MJFR1 ($n = 3$, nine measurement fields per replicate; data points: interreplicate mean of randomly matched fields). Iso3 is more persistent than iso1. *P* values of the group differences were calculated using *t* test. (**F**) Solid-state NMR hNH experiments of fully protonated iso1 and iso3 showing that they correspond to two distinct amyloid polymorphs at a local level. ppm, parts per million.

during fibrillization or a preexisting process, possibly stochastic as well, having formed several distinct soluble progenitors before sample splitting and subsequent fibrillization. If the latter did hold true, then one would have to also assume that during sample splitting, the progenitors would have been heterogeneously sorted into the different tubes. This could occur only under conditions of extreme dilution with only a few individual molecules of progenitors present in the sample. While this heterogenous sorting of preformed progenitors during sample splitting seems unlikely, it cannot be ruled out. This does not exclude, however, the development of a secondary stochastic process taking place during the fibrillization step as well.

In any case, with regard to the current methodological guidelines (*27*), these results argue against the exclusive use of ThT to monitor α-syn amyloids: This practice can lead to the conclusion that damped or null fluorescence rates of change correspond to "inhibited" or failed fibrillizations, while they can, in fact, reflect the emergence and growth of τ^- polymorphs. This can, for instance, become a substantial concern when studying drug candidates aimed at inhibiting fibrillization. The generalized practice of upstream screening fibrillization products with ThT also resulted in the artificial orientation of structural studies toward a restricted subset of α-syn amyloid structures excluding τ^- polymorphs [e.g., (*17*)].

A simple assay to resolve τ^- α-syn polymorphs

We thus decided to build a structural assay capable of discriminating between τ^- and regular ThT-positive polymorphs and to monitor amyloid species generation. The absence of ThT signal in the iso3 fibrils could be due to only subtle changes in the ThT-binding region of the assemblies. ThT is considered to bind to the outer surface of the amyloid assemblies, parallel to the main fibril axis. The binding site is different from the one occupied by Congo red and its derivatives like X-34 (*31*). With regard to the different amyloid folds adopted by α-syn in iso3 and iso1 (fig. S2), differences in the outer exposure of the C and N termini at each amyloid stack level can be hypothesized. This could have an impact on the accessibility of ThT to its binding site, on the affinity of the probe for the site, on the fluorescence of the bound probe due to the electrophilic environment, or a combination of these factors.

Thus, we hypothesized that fluorescent compounds with a slightly different chemical structure, but sharing with ThT its trimethine cyanine skeleton (*34*, *35*), could detect iso3. Notably, SYBR Green, the well-known DNA intercalating dye (Fig. 3A), was capable of sensing the amyloid structure of iso3 but appeared to be much less capable of doing so for iso1, giving an almost mirror image of the ThT readings: Iso1 was ThT-high and SYBR Green–low, while iso3 was ThT-low and SYBR Green–high (Fig. 3B). In contrast, the fluorescent Congo red derivative X-34, which binds to a distinct region in amyloids (*31*, *36*), detected iso1 and iso3 with a similar sensitivity (Fig. 3B): X-34 provided a polymorphism-independent readout of the total amounts of amyloids in each sample. Thus, as with prion strains and luminescent conjugated polymers (LCPs) (*37*), multiple external probing using these different molecules could discriminate the α-syn polymorph identities revealed by solid-state NMR. We therefore combined these probes into a multiplex assay to derive a fingerprint of the emerging α-syn assemblies at high throughput and termed it the "fibrilloscope" (Fig. 3C), a simple assay with four readouts: the three dyes ThT, SYBR Green, and X-34 and the measurement of ultraviolet (UV) light attenuation to exploit Mie scattering and sense the emergence of particulate assemblies in the 30- to 300-nm-diameter range (*38*, *39*).

τ^- polymorphs are self-replicating

Using the fibrilloscope, we compared a second series of spontaneous fibrillizations with a series of fibrillizations seeded with 1% of untouched iso1 or iso3 (Fig. 4A). In this second round, we used α-syn monomers bearing a single S129A substitution to ascertain that the phosphorylated aggregates appearing during the subsequent assays in neurons would correspond to assemblies newly formed at the expense of the endogenous pool of α-syn and not to a phosphorylation of the exogenous seeds (fig. S1) (*27*, *28*). Both iso1 and iso3 were able to prompt the appearance and the buildup of amyloids in vitro in comparison with all the spontaneous fibrillizations, with iso1 being even more potent than iso3 (see the X-34 and UV light attenuation readouts) (Fig. 4B). Moreover, all the amyloids that developed in the presence of 1% of iso1 (iso1.1 to iso1.5) were ThT-high and SYBR Green–low, while all the amyloids observed in the tubes inoculated with 1% of iso3 (iso3.1 to iso3.5) were ThT-low and SYBR Green–high (Fig. 4B), corresponding to an exact reproduction of the parental fibrilloscope fingerprint (Fig. 3B). The iso1 and iso3 samples thus contained distinctive amyloid particles capable of imposing their own core structural arrangement on monomers by conformational templating, driving the assembly of daughter amyloid structures. Notably, the second-generation samples retained the exact biological activity of their parents, i.e., all the samples descending from iso1 were inactive on cortical neurons, and all the iso3 offspring triggered an extensive synucleinopathy (Fig. 4C). This indicated that after inoculation, amyloid particles proliferated and that they retained both the fold and the neuronal spread propensity of the parent assemblies.

To explore the sustainability of this particle proliferation, we performed a third round of simultaneous fibrillizations in which we compared a series of conditions inoculated with 1% of the second-generation fibrillization products (fig. S3). This resulted in third-generation amyloids that exhibited the same fibrilloscope fingerprint and the same specific bioactivity as their ancestors (Fig. 4D). These results indicate that the novel τ^- polymorph iso3 is capable of replicating its distinctive amyloid fold with the same fidelity and sustainability as iso1, a prototypical ThT-positive type 2 polymorph species member (fig. S2) (*18*).

Acute neuronal spread of τ^- polymorphs: Cytopathological and neuroanatomical traits

We then looked more closely at the neuronal seeding activity of the different amyloid species that emerged in our experiments. First, we tried to determine why the iso1 strain members, already described as belonging to the type 2 polymorph species (*18*) and which proliferated most efficiently in vitro, were unable to spread in neurons. First, we observed that iso1 was cleared more rapidly than iso3 by neurons (Fig. 2D), suggesting that fewer iso1 seeds would remain available intracellularly to trigger a secondary fibrillization. In addition, previous studies concerning this polymorph (*23*) were indirectly suggestive of the existence of a monomer concentration threshold for conformational templating. We thus reasoned that these limitations could be overcome by forcing the mouse neurons to overexpress human α-syn, a condition that could favor the probability of interaction of more "templating-compatible" human monomers with the iso1 seeds. Notably, this overexpression was enough

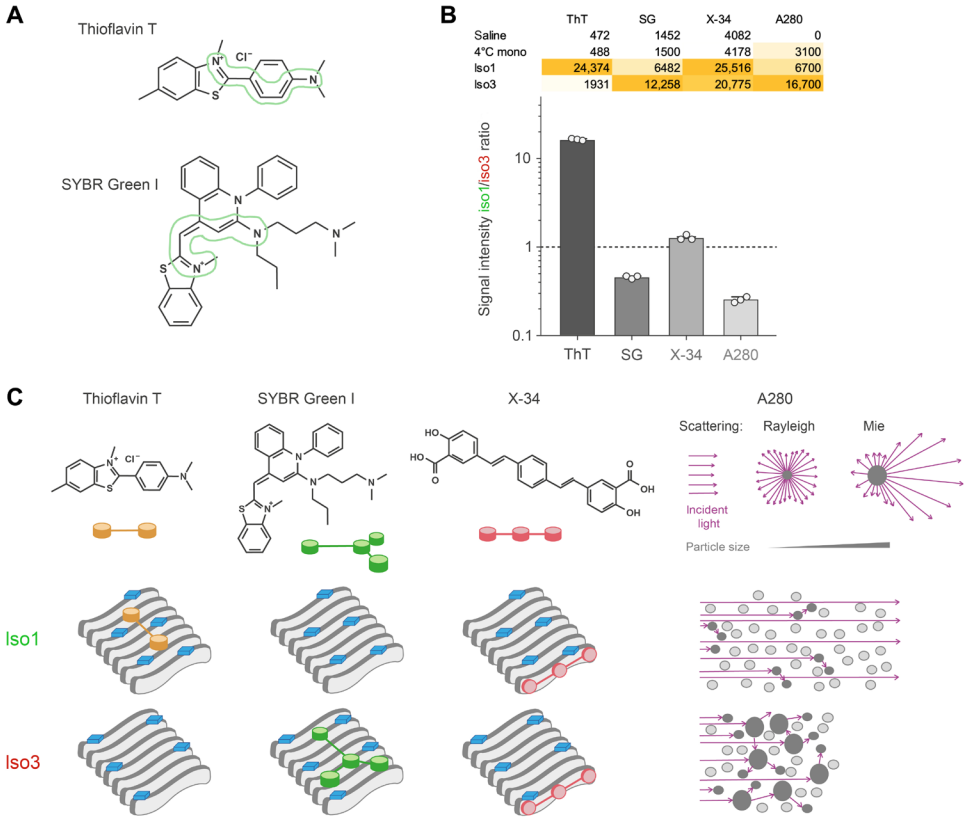

Fig. 3. A fibrilloscope for rapidly resolving τ⁻ polymorphs. (**A**) 2D structures of ThT and SG molecules showing their trimethine cyanine skeleton circled in green. (**B**) Fluorescence intensities of ThT, SG, and X-34, as well as light attenuation at 280 nm (A280) of iso1 versus iso3 samples (AU, table: mean of $n = 3$ measures). Ratios of iso1/iso3 signal intensities were calculated and plotted (bar graph) for each sample and probe, showing a specific detection of iso1 by ThT (more than five times higher than for iso3) and a specific detection of iso3 by SG (about two times higher than for iso1), and a higher light attenuation (almost five times), while detection with X-34 was similar for iso1 and iso3 ($n = 3$ measures). (**C**) Cartoon model of ThT, SG, and X-34 interaction of iso1 (top) and iso3 (bottom schemes). Putative identical exposed residues are depicted in blue bricks, showing a distinct quaternary structure of iso1 and iso3 assemblies affecting the behavior of the different probes under illumination. The A280 light attenuation difference between iso1 and iso3 is explained by the different relative contributions of Rayleigh (small particles, <30 nm) and Mie (larger particles with diameter from 30 to 300 nm) scattering by the assemblies composing iso1 and iso3.

to rescue the bioactivity of iso1 to a level comparable to that of iso3 (Fig. 5A). In addition, comparative mass spectrometry (MS) analysis of the neuronal assemblies that formed under these conditions indicated that endogenous mouse α-syn was excluded from the neoaggregates elicited by iso1.1, while those sparked by iso3.1 contained both human and mouse α-syn (Fig. 5, B and C). Thus, beyond a monomer concentration threshold and a fast clearance of the exogenous seeds, the inability of the iso1 family members to replicate in mouse neurons was probably also associated with a defective templating of mouse α-syn monomers compared to a more "natural" templating of human α-syn monomers, i.e., this was suggestive of a host-species specificity of the templating process for iso1.

In addition to iso3, we identified by serendipity a second τ⁻ polymorph, which we named "1B." It was also obtained by spontaneous generation in saline (fig. S3). Similar to iso3, this species was ThT-negative and was able to induce an extensive synucleinopathy in mouse cortical neurons (fig. S4). However, from a qualitative point of view, the synucleinopathy induced by 1B was characterized by many linear α-syn aggregates in the lumen of the neuronal processes and by the occasional presence of a single v-shaped or crisscrossed α-syn aggregate embedded in the nuclear chromatin of certain neurons (Fig. 5, D and E). In comparison, the synucleinopathy induced by iso3 was characterized by the frequent presence of cytoplasmic round or fuzzy α-syn aggregates located in the soma and of few linear structures in the processes, while intranuclear aggregates were never observed in this case (Fig. 5, D and E). The ability to induce these specific patterns was inheritable among seed generations (parents, first generation; children, second generation; and grandchildren, third generation) and constituted distinctive sustainable traits (Fig. 5, D and E). This indicates that as with the type 1 and type 2 polymorph families that have been previously well characterized (*14*–*18*), τ⁻ polymorphs are also populated by structurally distinct subfamilies, endowed with distinctive and inheritable replication patterns in neurons.

With regard to the florid neuritic synucleinopathy triggered by the τ⁻ polymorph 1B in cultured neurons, we reasoned that this τ⁻ polymorph could be particularly prone to trigger a synucleinopathy spreading over long distances along interconnected brain regions in vivo (*40*). Ten wild-type (WT) mice were unilaterally injected at the level of the substantia nigra pars compacta, with the τ⁻ polymorph 1B, and 10 sham-injected controls were performed in parallel (fig. S5A). Four months after the injection, secondary α-syn aggregates were selectively found in the soma of neurons located in the ipsilateral dorsal striatum of the 1B-injected animals, indicating that the

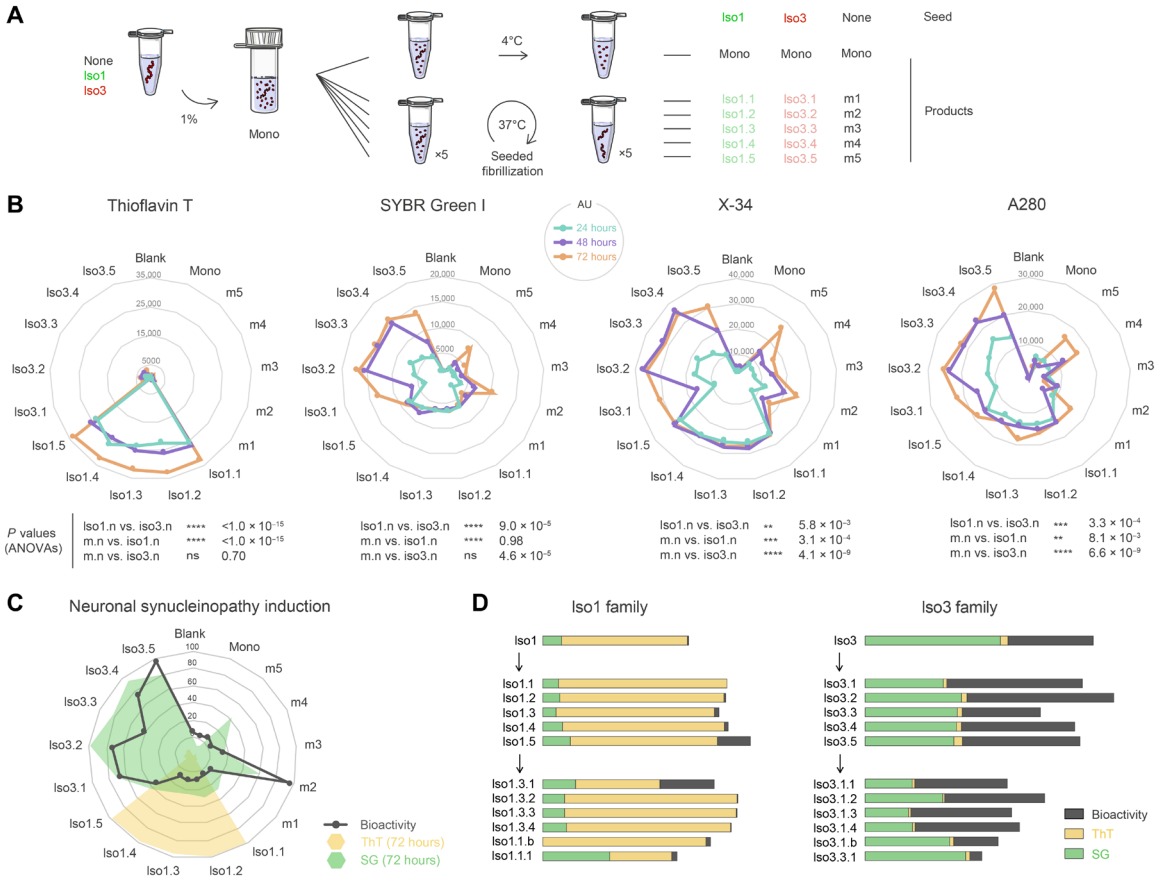

Fig. 4. The τ⁻ polymorph iso3 is the founder of a new strain. (**A**) Schematic representation of the secondary fibrillizations, with and without inoculation, and corresponding nomenclature. (**B**) Radar plots showing for each tube the intensity values of ThT, SG, X-34, and A280 at 24, 48, and 72 hours during the fibrillization process. The *P* value of the difference observed with each probe for the different fibrillization groups (1% iso1; 1% iso3; none; $n = 5$ for each group) was calculated using two-way analysis of variance (ANOVA) with Tukey correction. Distinctive kinetics indicative of seeded aggregation and speciation can be appreciated. (**C**) Radar plot of the extent of the synucleinopathic spread sparked by the 72-hour secondary fibrillization products in primary cultures of mouse cortical neurons. The latter HCA neuronal bioactivity tests were all run simultaneously, and each individual value plotted in the radar corresponds to the mean of 27 neuronal field quantifications made in three replicate culture wells. The corresponding 72-hour ThT and SG values already shown in (B) are superimposed for facilitating the appreciation of correlations. (**D**) Inheritance of specific ThT, SG, and bioactivity traits across seed generations. In this graph, all three parameter values were divided for each single sample by its X-34 value to normalize the parameters with respect to the total amyloid load characterizing each sample. The latter normalization was not shown in the title blocks for the sake of simplicity. The statistical significance of the intergeneration (children versus grandchildren for each group) and intergroup (iso1 versus iso3 for each generation) differences was determined using the Hotelling's T^2 test with Bonferroni's correction for multivariate analysis simultaneously exploiting the three parameters characterizing every sample: iso1 children versus iso1 grandchildren, $P = 0.70$; iso3 children versus iso3 grandchildren, $P = 0.84$; iso1 children versus iso3 children, $P < 10^{-15}$; and iso1 grandchildren versus iso3 grandchildren, $P = 0.012$. ns, not significant.

synucleinopathy propagated between interconnected brain regions (fig. S5, A to D). The rostral pattern of spread was generally consistent between animals. In some cases, however, the synucleinopathy also spread to the insular cortex and to the core of nucleus accumbens, suggesting transmission from the ventral tegmental area as well (fig. S5B). In agreement with our observation in cultured neurons, the synucleinopathy triggered by 1B resulted not only in the appearance of numerous somatic and neuritic aggregates (fig. S5, B to D) but also in neuronal nuclear inclusions (fig. S5, E to G).

τ⁻ polymorphs proliferate and perpetuate their fold in neurons

These results prompted us to determine whether the aggregates that were newly formed in neurons exposed to τ⁻ polymorphs were conformational replicas of the exogenous seeds: in other words, whether they resulted from a bona fide conformational templating. To proceed with a comparative analysis of the τ⁻ polymorph iso3 and of its neuronal propagation products, we first tried to identify distinctive immunological and physicochemical features that could differentiate iso3 from the regular type 2 polymorph iso1 (*14*, *18*) and that could be used to characterize the newly formed assemblies (Fig. 6). In that respect, we observed that the two types of amyloid particles isolated by density floatation exhibited different affinities for the conformation-dependent antibody Syn-F1. The staining of iso1 was much weaker than that of the τ⁻ polymorph iso3 (Fig. 6A). To determine whether this feature was inheritable, we put the daughter amyloid particles iso1.1 and iso3.1 and the grandchild particles iso1.1.1 and iso3.1.1 under scrutiny. After simple trapping on nitrocellulose and aldehyde fixation, we found that the two particle species

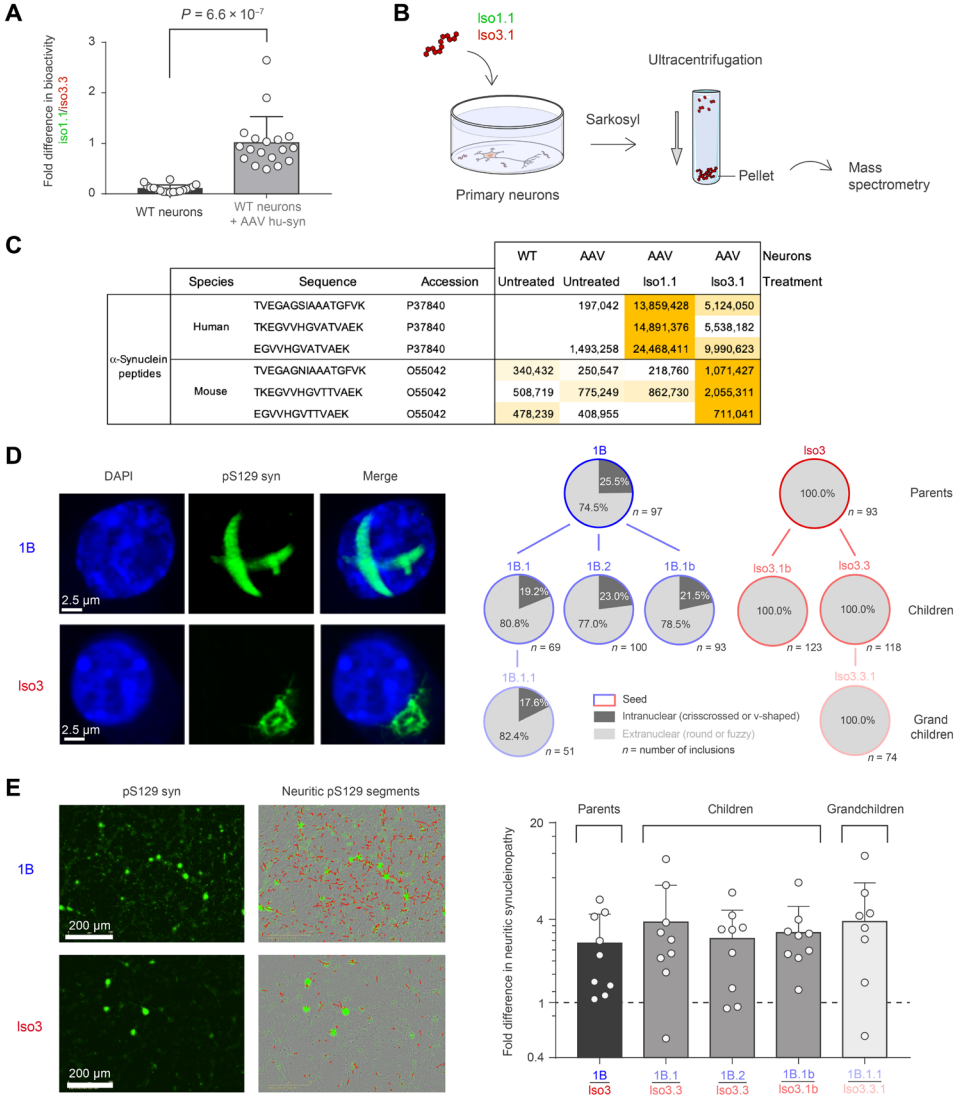

Fig. 5. The reference ThT-positive polymorph iso1 needs human α-syn overexpression to demonstrate a bioactivity, while the τ⁻ polymorphs iso3 and 1B trigger distinctive subcellular spread patterns in naïve mouse neurons. (**A**) Neuronal synucleinopathic spread initiated by iso1 and iso3 in naïve and human α-syn overexpressing mouse neurons [see also (C)]. *P* value of the difference in bioactivity observed for the groups ($n = 18$ for each group) was calculated using a *t* test. (**B**) Schematic representation of the extraction analysis of insoluble proteins from neurons treated with iso1 and iso3 as in (A). (**C**) Pellets from (B) were analyzed by MS. Three peptides specific to mouse α-syn, three specific to human α-syn, and five common to both species were identified by MS. The species, sequence, and hit counts are represented in the table, as well as their sums, represented in the master protein rows. (**D**) Left images show typical somatic α-syn inclusions that beacon the experimental synucleinopathy triggered by iso3 and 1B in our HCA assay (scale bars, 2.5 μm). Right quantifications show that the intranuclear crisscrossed inclusions are distinctive of the synucleinopathy triggered by 1B and its offspring. The counts correspond to the number of somatic aggregates detected in 18 standardized image acquisition fields for each condition. (**E**) Left images show the extended neuritic synucleinopathy (and its analytical segmentation) caused by 1B compared to iso3 in the neuronal HCA assay. Right quantifications show the 1B/iso3 activity ratio with respect to the induction of neuritic synucleinopathy: This ratio appears to be a constant among all the particle generations produced from 1B and iso3; $n = 9$ for each group; the individual ratio values correspond to the ratio of random pairs of 1B group and iso3 group measurements. AAV, adeno-associated virus; DAPI, 4′,6-diamidino-2-phenylindole.

indeed exhibited inheritance of their level of sensitivity toward Syn-F1 (Fig. 6B and fig. S6). Note that the conformational epitope recognized by Syn-F1 partially maps to the C terminus of α-syn. Although the C terminus does not participate in the amyloid stack, it is likely that the topology of the amyloid fold that involves upstream regions of the protein still determines its level of exposure, its orientation, and probably its dynamics at the periphery of the fibrillar axis. Depending on the polymorph, aldehyde fixation could thus "freeze" the C terminus in different positions at the surface of the fibrils. This could account for the differential binding of Syn-F1 to iso1 and iso3.

We next focused on iso1.1 and iso3.1 and added two upstream steps (i) harsh treatment with sarkosyl, mimicking the extraction and recovery procedures of insoluble α-syn amyloids from neurons, and (ii) velocity sedimentation for size separation. These additional steps completely abolished the Syn-F1 immunoreactivity of iso1.1,

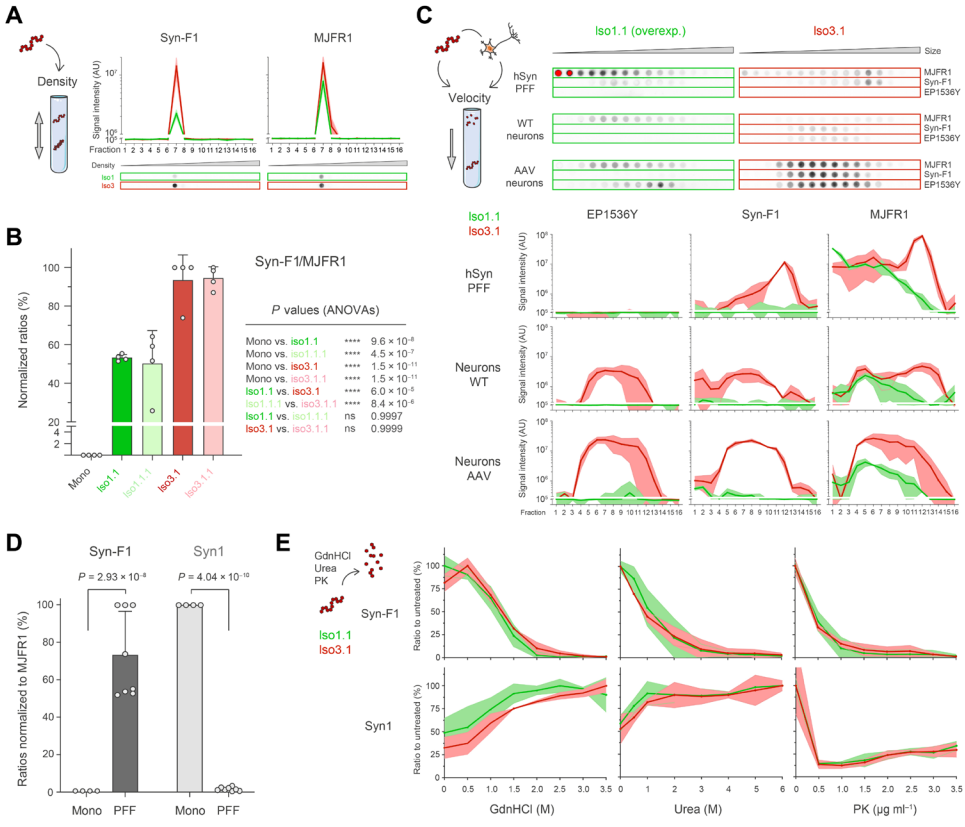

Fig. 6. The τ⁻ polymorph iso3 perpetuates its fold in living neurons. (**A**) Density floatations of iso1 and iso3. Fractions filter-trapped and analyzed with Syn-F1 and MJFR1 ($n = 3$). Mean curves, bold lines; SD, shaded areas. (**B**) α-syn monomers (gray), iso1.1 (dark green), iso1.1.1 (light green), iso3.1 (dark red), and iso3.1.1 (light red) filter-trapped and revealed as in (A). Syn-F1 to MJFR1 ratio plotted in a bar graph with individual $n = 4$ samples per group. *P* values were calculated with two-way ANOVA with Tukey correction. (**C**) Velocity sedimentations of iso1.1 (green) and iso3.1 (red) and of extracts from primary neurons (WT or AAV-hSyn–infected) treated with iso1.1 or iso3.1. The fractions were filter-trapped and revealed with MJFR1, Syn-F1, and EP1536Y (top, representative immunoblots). Top: Iso1.1 PFF conditions are overexposed compared to iso3.1 to allow better visualization. Graphs show the quantification from $n = 3$ replicates per group of the absolute chemiluminescence signal (AU). Data presented are the mean curves (bold lines) with SDs (lighter shaded areas). (**D**) Filter trap of monomeric and α-syn fibrils revealed with Syn-F1, Syn1, and MJFR1. Ratios of Syn-F1 and Syn1 to MJFR1 are plotted in a bar graph with individual $n = 4$ and $n = 8$ for monomers and fibrils, respectively. Multiple *t* tests, Holm-Sidak corrected for multiple comparisons, gave the indicated *P* values reflecting a specific immunoreactivity of α-syn fibrils and monomers toward Syn-F1 and Syn1, respectively. (**E**) Iso1.1 (green) and iso3.1 (red) were subjected to guanidinium (GdnHCl), urea, and PK treatments [0 to 3.5 M GdnHCl, 1 hour, 25°C; 0 to 6 M urea, 6 hours, 25°C; and PK (0 to 3.5 μg/ml), 30 min, 37°C]; reaction aliquots were then filter-trapped and revealed with Syn-F1 (fibrillar, top graphs) or Syn1 (monomers, bottom graphs) ($n = 3$). Representative immunoblots are shown in fig. S6.

while that of iso3.1 was preserved, further widening the "immunoreactivity gap" between the two species (Fig. 6C).

In the gradients of Fig. 6C, the MJFR1 antibody (human α-syn–specific) selectively detected the exogenous seeds and permitted their fate to be followed 3 weeks after treatment [see "PFF" (preformed fibril) and "WT neurons" rows]. EP1536Y, on the other hand, specifically detected the seeded newly formed amyloid aggregates. By comparing the results obtained with the two stains, it appears that neurons progressively clear the exogenous fibrils ("MJFR1" column) and that the amyloids that newly replicate inside neurons ("EP1536Y" column) span a shorter size range compared to the input fibril seeds. As to the conformation-specific antibody Syn-F1, as one could have expected at this point, the newly formed α-syn assemblies that proliferated inside the neurons expressing human α-syn also inherited the specific all-or-none Syn-F1 immunoreactivity of the seed species used to inoculate the cultures (Fig. 6C and fig. S6). This indicated that "seed species"–specific templated growth occurred during propagation inside living neurons for both the regular type 2 polymorph iso1 (*14*, *18*) and for the τ⁻ polymorph iso3.

Note that, apart from its solid-state NMR and fibrilloscope fingerprints and distinctive reactivity of its Syn-F1 epitope, the τ⁻ polymorph iso3 was otherwise undistinguishable from iso1 with respect (i) to its sensitivity to proteinase K (PK), (ii) to its resistance to urea or guanidinium chloride (Fig. 6, D and E), and (iii) to its gross fibrillary appearance (Fig. 2D). This indicates that both the fibrilloscope fingerprint and the Syn-F1 epitope exposure identify subtle arrangements of the fibril surface not reflected "macroscopically" yet encode a size distribution pattern of the amyloid assemblies (Figs. 2C and 6C), a particle proliferation rate (Fig. 4B), and neuronal and cytopathological spread patterns (Fig. 5) that are distinctive of τ⁻ polymorphs.

DISCUSSION

Our study demonstrates that spontaneous and uncontrolled emergence of τ⁻ polymorphs with exacerbated neuronal spreading abilities can take place during the standard preparation of PFFs (*27*). This clearly begs the question as to whether the bioactivity characterizing PFF preparations could be partly due to the unsuspected presence

of these τ^- polymorphs. In that respect, it will be important to distinguish how much the increased pathology triggered by τ^- polymorphs in our study is due to its higher stability in mouse neurons versus a higher engagement with mouse α-syn per se. Note that despite a minor stability compared to iso3 (Fig. 2E), replication of iso1 is restored when mouse neurons overexpress human α-syn (Fig. 5A). This can be taken as an indication that engagement could be a greater determining factor here. This raises the question as to whether τ^- polymorphs can emerge in patients and contribute to the formation and spread of the cytopathological inclusions in synucleinopathies.

The ThT invisibility of τ^- polymorphs reported here could be taken as an indication that they are not the main components of these inclusions, as the latter consistently appears ThT positive in neuropathological studies. However, it should be kept in mind that our present ThT measurements concern native protein assemblies in saline and are both "bulk phase" and "no wash." This means that when detected, the ThT signals are above the fluorescence background of unbound ThT under conditions where the probed volume is represented at >99% by the solvent phase that properly contains unbound ThT. Under these conditions, τ^- polymorphs like iso3 exhibit a very low ThT signal that is ~10-fold smaller than that of iso1 yet is ~4-fold higher than the corresponding monomer condition (Fig. 2A). This fourfold change detected in our bulk phase conditions is likely to be sufficient to grant an apparent "ThT-positive" status to inclusions containing τ^- polymorphs under histopathological detection conditions. In histopathology, ThT staining is performed on aldehyde-fixed sections in which the protein assemblies are cross-linked and often treated with organic solvents and/or detergents. The ThT fluorescence images are then acquired after washing the unbound ThT fraction. In addition, imaging interrogates the sample in a pixelwise fashion, and thus, for the pixels located at the proper level of an inclusion, probably over 50% of the probed volume corresponds to the assembly itself. Thus, inclusions concentrating τ^- polymorphs should appear ThT positive over a darker background in histopathology. Note, however, that in neuropathological sections, the ThT difference between the τ^- and "regular" polymorphs might also be blunted because of a possible impact of fixation/organic solvents/detergents on the physicochemical topology of the fibrils.

Recent observations suggest that τ^- polymorphs might well emerge under diseased conditions. Reminiscent of the "ThT dichotomy" characterizing τ^- and regular α-syn polymorphs, α-syn fibrils amplified from the cerebrospinal fluid and postmortem brain extracts of patients with multiple system atrophy (MSA) are respectively ~3 and ~10 times less ThT positive than the ones amplified from comparable samples of patients with PD (*25*). The ThT dichotomy reported in (*25*) appears likely to correspond to the detection of distinct α-syn polymorphs, as the measurements with the HC-169 amyloid probe excluded a quantitative bias due to the amount of amyloids generated by the amplification procedure (*25*). In another study, α-syn fibrils amplified from brain extracts from different patients with PD and MSA also exhibited variable ThT intensities and stained differently with a set of external fluorescent probes (*41*).

From a cytopathological point of view, the τ^- polymorph 1B triggers a florid Lewy neurite pathology and the frequent formation of α-syn inclusions crisscrossing neuronal nuclei. This is intriguing since Lewy neurites are rather reminiscent of the neuropathological signs of PD, while the presence of neuronal nuclear inclusions is, instead, a very specific and early sign of MSA (*42*, *43*).

Collectively, these results justify further characterization of the molecular and supramolecular organization of τ^- polymorphs and the identification of their specific neuronal protein "interactome" compared to ThT-positive α-syn fibrils. This should aid in understanding the correlations that exist between the amyloid fold, the outer surface topology of the fibril polymorphs, and their specific interactions with the surrounding intraneuronal environment.

MATERIALS AND METHODS

α-syn expression

Escherichia coli strain BL21(DE3) plysS was transformed with pET24–α-syn vector by electroporation and plated onto Luria broth agar plate containing kanamycin (30 μg/ml). A preculture in 5 ml of Luria broth medium was inoculated with one clone and incubated at 37°C under 200 rpm shaking for 4 hours. The expression on α-syn was carried out in M9 minimal medium containing ^{13}C glucose (2 g/liter) and $^{15}NH_4Cl$ (1 g/liter) as carbon and nitrogen sources. Cells from the Luria broth preculture were recovered by centrifugation (1000*g*, 10 min) and used for inoculating 200 ml of M9 medium. Cells were grown overnight at 37°C under 200 rpm shaking and then diluted in 2 liters of culture. Protein expression was induced by adding 1 mM isopropyl-β-D-thiogalactopyranoside during exponential phase, evaluated at an optical density at 600 nm reaching 0.8. Cells were harvested after 4 to 5 hours of culture at 37°C by 6000*g* centrifugation (JLA 8.1, Beckman Coulter), and pellet was kept at −20°C before purification. The site-specific nonphosphorylatable mutant S129A was obtained by site-directed mutagenesis of pET24–α-syn.

α-syn purification

Pellet was thawed in 10 mM tris-HCl (pH 8.0), 1 mM EDTA, 1 mM phenylmethylsulfonyl fluoride, and Pierce EDTA-free protease inhibitor tablet (Thermo Fisher Scientific) buffer and sonicated three times for 45 s (Bandelin SONOPULS, VS70T probe) before centrifugation. The supernatant was boiled for 20 min and centrifuged. Streptomycin sulfate was added to the supernatant to a final concentration of 10 mg/ml, and the solution was stirred for 15 min at 4°C and then centrifuged. Ammonium sulfate was added to the supernatant to a final concentration of 360 mg/ml, and the mixture was stirred for 15 min at 4°C before centrifugation. These four centrifugations were performed at 20,000 rpm for 30 min and at 4°C with a Beckman Coulter JA-25.5 rotor. The pellet was resuspended in 25 mM tris-HCl (pH 7.70) and dialyzed against the same buffer to eliminate salts. The dialyzed sample was injected onto a HiTrap Q HP column previously equilibrated with 25 mM tris-HCl (pH 7.70), and α-syn was eluted around 250 μM NaCl by steps from 0 to 500 mM NaCl with an ÄKTA pure system. Fractions containing the protein were dialyzed against 20 mM tris-HCl (pH 7.40) and 100 mM NaCl buffer before loading onto a 75-pg HiLoad 26/600 Superdex column equilibrated with the same buffer with ÄKTA pure system. Monomeric fractions were collected and concentrated if needed by using Vivaspin 15R 2-kDa cutoff concentrator (Sartorius Stedim). Purification fractions were checked by using polyacrylamide gel electrophoresis (PAGE) tris-tricine 13% dying with ProBlue Safe Stain. Protein concentration was evaluated spectrophotometrically by using absorbance at 280 nm and extinction coefficient of 5960 M^{-1} cm^{-1}. Quantification of the preparations with a Pierce chromogenic LAL kit indicated a low endotoxin [lipopolysaccharide (LPS)] residual value: 0.03 to 0.06 EU per μg of recombinant protein (*44*).

α-syn fibrillization

Solutions of monomeric α-syn at 4 to 5 mg/ml in saline [H_2O, 100 mM NaCl, and 20 mM tris-HCl (pH 7.40)] were sterilized by filtration with 0.22-μm Millipore single-use filters and stored in sterile 15-ml conical falcon tubes at 4°C. Sterilized stock was then distributed into safe-lock Biopur individually sterile-packaged 1.5-ml Eppendorf tubes as 500-μl aliquots. The tubes were cap-locked and additionally sealed with parafilm. All previous steps were performed aseptically in a particle-free environment under a microbiological safety laminar flow hood. For comparative fibrillizations, all samples were loaded simultaneously in a ThermoMixer (Eppendorf) in a 24-position 1.5-ml Eppendorf tube holder equipped with a heating lid. Temperature was set to 37°C, and shaking was set to 2000 rpm. Sampling for measurements during the fibrillization process was done by temporarily returning the samples under the microbiological safety laminar flow hood. Raising LPS by exogenous addition from the residual value of ~0.018 to 100 μg/ml did not favor the appearance of ThT-positive assemblies under these fibrillization conditions (*21*).

Amyloid probes and fibrilloscope measurements

Samples from the fibrillized α-syn aliquots or of the control α-syn monomers stored at 4°C were diluted to 0.1 mg/ml in 100 μl of phosphate-buffered saline (PBS) containing either 20 μM ThT, 20 μM X-34, 0.1% SYBR Green I (SG) commercial stock solution, or nothing else. The diluted samples were distributed either in 96-well plates (samples with probes) or in UVettes (Eppendorf) (samples without probe). After 20 min at room temperature protected from ambient light, the plates were read under orbital shaking in a BMG LABTECH FLUOstar OPTIMA fluorimeter. Excitation/emission wavelength pairs were 380 nm/520 nm for X-34, 450 nm/480 nm for ThT, and 485 nm/520 nm for SG. The UVettes were read at 280 nm using the 1-cm optical path with an Eppendorf biophotometer in absorbance mode to generate the A280 light attenuation readout.

Sonication and NTA

Samples from the fibrillized α-syn aliquots or of the control α-syn monomers stored at 4°C were diluted to 0.1 mg/ml in 100 μl in PBS and distributed in cap-locked, sterile 0.5-ml polymerase chain reaction (PCR) tubes (Thermo Fisher Scientific). When relevant, sonication was performed at 25°C in a Bioruptor Plus water bath sonicator (Diagenode) equipped with thermostatic control and automated tube carousel rotator. The sonication power was set to "high," and 10 cycles of 30-s "on" followed by 10-s "off" were applied. The impact of this sonication protocol on the particle contents of the samples was scored using an NanoSight NS300 NTA platform (Malvern) (see Fig. 1D).

HCA of experimental synucleinopathy in neurons

Timed pregnant C57BL/6J female mice were received from Charles River Laboratories 2 days before initiation of the primary culture. The cultures were synchronized with the α-syn fibrillizations to use untouched amyloids in the bioassay. Cortices were harvested from embryonic day 18 mouse embryos and dissociated enzymatically and mechanically (using neural tissue dissociation kit, C Tubes, and an Octo Dissociator with heaters; Miltenyi Biotech, Germany) to yield a homogenous cell suspension. The cells were then plated at 20,000 per well in 96-well plates (Corning, BioCoat poly-D-lysine imaging plates) in neuronal medium (MACS Neuro Medium, Miltenyi Biotech, Germany) containing 0.5% penicillin-streptomycin, 0.5 mM alanyl-glutamine, and 2% NeuroBrew supplement (Miltenyi Biotech, Germany). The cultures were maintained with 5% CO_2 at 37°C in humidified atmosphere. The medium was changed by one-third every 3 days, until a maximum of 30 DIV (days in vitro). In such cultures, and under control conditions, neurons represented approximately 85 to 95% of the cell population; thus, in the text and for the sake of simplicity, they are referred to as "neurons." After 7 DIV, vehicle and α-syn amyloid–containing samples were added at a final concentration of 10 nM equivalent monomeric concentration. When relevant, neurons were infected at DIV 10 with α-syn AAV (adeno-associated virus) particles (multiplicity of infection, 1000). All antibodies used and shown in the study are summarized in table S1. For live-dead analysis, DIV 30 cultures were loaded with 1 μM calcein-AM for 30 min at 37°C, the plates were washed with Hanks' balanced salt solution (pH 7.4), and the de-esterified calcein retained in the living neurons was immediately imaged using Incucyte S3.

Human α-syn AAV particles

Recombinant AAV9-CMVie/SynP-wtsyn-WPRE vector containing the sequence of human α-syn put under control of the human synapsin promoter was produced by polyethylenimine-mediated triple transfection of low-passage human embryonic kidney–293T/17 cells (American Type Culture Collection; catalog number CRL-11268). The AAV expression plasmid pAAV2-CMVie/hSyn-wtsyn-WPRE-pA was cotransfected with the adeno helper pAd Delta F6 plasmid (Penn Vector Core, catalog number PL-F-PVADF6) and AAV Rep Cap pAAV2/9 plasmid (Penn Vector Core, catalog number PL-T-PV008). Cells are harvested 72 hours after transfection, resuspended in lysis buffer [150 mM NaCl and 50 mM tris-HCl (pH 8.5)], and lysed by three freeze-thaw cycles (37°C/−80°C). The cell lysate was treated with Benzonase (150 U/ml; Sigma-Aldrich, St. Louis, MO) for 1 hour at 37°C, and the crude lysate was clarified by centrifugation. Vectors are purified by iodixanol step gradient centrifugation and concentrated and buffer-exchanged into lactated Ringer's solution (Baxter, Deerfield, IL) using Vivaspin 20 100-kDa cutoff concentrator (Sartorius Stedim, Göttingen, Germany).The genome-containing particle titer was determined by quantitative real-time PCR using the LightCycler 480 SYBR Green Master mix (Roche, catalog number 04887352001) with primers specific for the AAV2 inverted terminal repeats (forward, 5′-GGAACCCCTAGTGATGGAGTT-3′ and reverse, 5′-CGGCCTCAGTGAGCGA-3′) on a LightCycler 480 instrument. Purity assessment of vector stocks was estimated by loading 10 μl of vector stock on 10% SDS acrylamide gels, and total proteins were visualized using the Krypton Infrared Protein Stain according to the manufacturer's instructions (Life Technologies).

Preparation of α-syn amyloid assemblies from pure protein samples and from neurons for analytical centrifugations

Stock preparations of amyloid fibrils [4 to 5 mg/ml in tris-buffered saline (TBS)] were diluted to a final concentration of 0.1 mg/ml in TBS. The equivalent of the quantity of recombinant human α-syn fibrils used for the treatment of one petri dish of primary neurons (1.66 μg) was diluted in 500 μl of final volume with solubilization buffer (SB): 10 mM tris (pH 7.5), 150 mM NaCl, 0.1 mM EDTA, 1 mM dithiothreitol, cOmplete EDTA-free protease inhibitors (Roche), and PhosSTOP phosphatase inhibitors (Roche), with a final concentration of 1% (w/v) *N*-lauroyl-sarcosine (sarkosyl, Sigma-Aldrich),

2 mM $MgCl_2$, and Benzonase nuclease (~0.5 U/μl; Millipore). For treated primary neuron solubilization, 500 μl of SB was added per petri dish at room temperature. Cells were scraped with a scraper before transferring the lysate in a 1.5-ml centrifuge tube. Fibrils or primary neuron lysates were then solubilized by incubating at 37°C under constant shaking at 600 rpm (ThermoMixer, Eppendorf) for 45 min.

Velocity sedimentation and density floatation gradients

Sedimentation velocity and density floatation gradient fractionations were performed as previously published (*32*). Briefly, for velocity sedimentations, a volume of 400 μl was loaded on top of an 11-ml continuous 10 to 25% iodixanol gradient [OptiPrep, 60% (w/v) iodixanol, Sigma-Aldrich] in SB with 0.5% (w/v) sarkosyl linearized directly in ultracentrifuged 12-ml tubes (Seton) with a Gradient Master (Biocomp). For density floatation gradients, 400 μl of solubilized material was diluted in SB with 50% iodixanol and 0.5% (w/v) sarkosyl to make a final concentration of 40% iodixanol. This sample-containing cushion was loaded within an 11.4-ml 10 to 60% discontinuous iodixanol gradient in SB with 0.5% (w/v) sarkosyl. The gradients were centrifuged at 200,000*g* for 2.5 hours at room temperature (velocity) or at 180,000*g* for 16 hours at 4°C (density) in a swinging-bucket SW-41 Ti rotor using an Optima LE-80K ultracentrifuge (Beckman Coulter). Gradients were then segregated into 16 equal fractions from the top using a piston fractionator (Biocomp) and a fraction collector (Gilson). Fractions were aliquoted for further analysis of their content by dot blot, immunoblot on SDS-PAGE, or native PAGE. Gradient linearity was verified by refractometry.

Analysis of the protein contents of velocity and density fractions by filter trap

For filter trap assays, native fractions were spotted onto nitrocellulose 0.2-μm membranes (Protran, GE) using a dot blot vacuum device (Whatman). Nitrocellulose membranes were fixed for 30 min in PBS with paraformaldehyde (PFA) at 0.4% (v/v) (Sigma-Aldrich) final concentration. After three washes with PBS, membranes were blocked with 5% (w/v) skimmed powder milk in PBS-Tween 0.5% (v/v) and probed with primary and secondary antibodies in PBS-Tween with 4% (w/v) bovine serum albumin (table S1). Immunoreactivity was visualized by chemiluminescence (Bio-Rad). The amount of the respective protein in each fraction was determined by the Image Studio Lite software after acquisition of chemiluminescent signals with a ChemiDoc digital imager (Bio-Rad). The profiles obtained were normalized and plotted with SD, all with respective Student's *t* test and analysis of variance (ANOVA) using the Prism software.

Extraction of insoluble proteins from PFF-treated primary neurons for MS

Fibril-treated primary neuron lysates were prepared from a petri dish as previously described for velocity and density gradients. For extraction of insoluble proteins, 500 μl of solubilized lysates were mixed 1:1 with SB 40% (w/v) sucrose, without sarkosyl, $MgCl_2$, and Benzonase, in 1-ml thickwall polycarbonate ultracentrifuge tubes (Beckman Coulter) and centrifuged at 250,000*g* for 1 hour at room temperature with a TLA 120.2 rotor using an Optima XP benchtop ultracentrifuge (Beckman Coulter). Supernatants were collected by pipetting. Pellets were resuspended in 50 μl of PBS, and total protein concentration was determined by bicinchoninic acid assay (Pierce) before equalization and denaturation for 5 min at 100°C in Laemmli buffer.

Mass spectrometry

Sample preparation and protein digestion

Ten micrograms of total protein per sample was deposited onto SDS-PAGE gel for concentration and cleaning purpose. Separation was stopped once proteins have entered the resolving gel. After colloidal blue staining, bands were cut out from the SDS-PAGE gel and subsequently cut into 1 mm by 1 mm gel pieces. Gel pieces were destained in 25 mM ammonium bicarbonate/50% acetonitrile (ACN), rinsed twice in ultrapure water, and shrunk in ACN for 10 min. After ACN removal, gel pieces were dried at room temperature, covered with the trypsin solution (10 ng/μl in 50 mM NH_4HCO_3), rehydrated at 4°C for 10 min, and lastly incubated overnight at 37°C. Spots were then incubated for 15 min in 50 mM NH_4HCO_3 at room temperature with rotary shaking. The supernatant was collected, and an H_2O/ACN/HCOOH (47.5:47.5:5) extraction solution was added onto the gel slices for 15 min. The extraction step was repeated twice. Supernatants were pooled and dried in a vacuum centrifuge. Digests were lastly solubilized in 0.1% HCOOH.

Nanoliquid chromatography–tandem MS analysis and label-free quantitative data analysis

Peptide mixture was analyzed on an UltiMate 3000 Nano LC system (Dionex) coupled to an Electrospray Orbitrap Fusion Lumos Tribrid mass spectrometer (Thermo Fisher Scientific). Ten microliters of peptide digests was loaded onto a 300-μm–inner diameter × 5-mm C18 PepMap trap column (LC Packings) at a flow rate of 10 μl/min. The peptides were eluted from the trap column onto an analytical 75-mm–inner diameter × 50-cm C18 PepMap column (LC Packings) with a 4 to 40% linear gradient of solvent B in 105 min (solvent A was 0.1% formic acid, and solvent B was 0.1% formic acid in 80% ACN). The separation flow rate was set to 300 nl/min. The mass spectrometer operated in positive ion mode at a 1.8-kV needle voltage. Data were acquired using Xcalibur 4.1 software in data-dependent mode. MS scans [mass/charge ratio (*m/z*), 375 to 1500] were recorded at a resolution of $R = 120{,}000$ (at *m/z* of 200) and an AGC target of 4 × 105 ions collected within 50 ms. Dynamic exclusion was set to 60 s, and top speed fragmentation in HCD mode was performed over a 3-s cycle. Tandem MS scans with a target value of 3 × 103 ions were collected in the ion trap with a maximum fill time of 300 ms. In addition, only +2 to +7 charged ions were selected for fragmentation. Other settings were as follows: no sheath or auxiliary gas flow; heated capillary temperature, 275°C; normalized HCD collision energy of 30%; and an isolation width of 1.6 *m/z*. Monoisotopic precursor selection was set to peptide, and an intensity threshold was set to 5 × 103.

Database search and results processing

Data were searched by SEQUEST through Proteome Discoverer 2.3 (Thermo Fisher Scientific) against the *Mus musculus* Reference Proteome Set (from UniProt 2019-07; 55,121 entries). Spectra from peptides higher than 5000 Da or lower than 350 Da were rejected. The search parameters were as follows: Mass accuracy of the monoisotopic peptide precursor and peptide fragments was set to 10 parts per million and 0.6 Da, respectively. Only b-ions and y-ions were considered for mass calculation. Oxidation of methionines (+16 Da) and protein N-terminal acetylation (+42 Da) were considered as variable modifications, and carbamidomethylation of cysteines

(+57 Da) was considered as fixed modification. Two missed trypsin cleavages were allowed. Peptide validation was performed using Percolator algorithm, and only "high confidence" peptides were retained corresponding to a 1% false-positive rate at peptide level. Peaks were detected and integrated using the Minora algorithm embedded in Proteome Discoverer. Proteins were quantified on the basis of unique peptide intensities. Normalization was performed on the basis of total protein amount. Protein ratios were calculated as the median of all possible pairwise peptide ratios. A *t* test was calculated on the basis of background population of peptides or proteins. Quantitative data were considered for proteins quantified by a minimum of two peptides, fold changes above two, and a statistical *P* value lower than 0.05.

Measurements of the resistance of fibrils to disassembly, denaturation, and proteolysis

Fibril stock preparations (4 to 5 mg/ml in TBS) were diluted to a final concentration of 0.1 mg/ml in TBS. For each guanidine hydrochloride (guanidinium, GdnHCl; Sigma-Aldrich), urea (Sigma-Aldrich), and PK (Sigma-Aldrich) concentration, 10 µl (1 µg) of PFF was mixed 1:1 with 10 µl of stock solutions to make 0, 0.5, 1, 1.5, 2, 2.5, 3, and 3.5 M GdnHCl final concentrations; 0, 0.5, 1, 2, 3, 4, 5, and 6 M urea final concentrations; and 0, 0.5, 1, 1.5, 2, 2.5, 3, and 3.5 µg/ml PK final concentrations. Mixtures were gently vortexed before incubation for 1 hour at room temperature for GdnHCl, 6 hours at room temperature for urea, and 30 min at 37°C for PK. At the end of the incubation period, treatments were stopped by quickly diluting the samples with 500 µl of PBS and directly subjecting them (100 µl per immunoblotting antibody) to filter-trap assay as previously described. The different α-syn species were quantified by immunolabeling with conformation-specific, monomeric, or pan α-syn antibodies (table S1) and expressed as a percentage of related untreated samples, allowing to draw curves of PFF disassembly, denaturation, and proteolysis with GdnHCl, urea, and PK, respectively.

In vivo experimental synucleinopathy

Adult male C57BL/6 mice were bred at the Institute of Lab Animal Science (Chinese Academy of Medical Sciences, Beijing, China). All mice were housed in a temperature-controlled (22°C) and light-controlled environment on a 12-hour light/12-hour dark cycle at the Institute of Lab Animal Science animal care facility with access to food and water ad libitum. The study design was approved by the Institute of Lab Animal Science Institutional Animal Care And Use Committee (Chinese Academy of Medical Sciences, Beijing, China), and all experimental procedures were conducted in accordance with the European Communities Council Directive (2010/63/EU) for care of laboratory animals in an AAALAC-accredited facility. The mice (2 months old) unilaterally received 2 µl of sonicated τ^- polymorph α-syn fibrils 1B (2.5 mg/ml) by stereotactic delivery to the region immediately above the right substantia nigra (coordinates from bregma: AP, −2.9; L, −1.3; DV, −4.5) at a flow rate of 0.4 µl/min, and the pipette was left in place for 5 min after injection to avoid leakage. Animals were euthanized after 4 months. Ten mice were used in each group, with male and female mixed. The brains were perfused with saline, postfixed for 3 days in 10 ml of 4% PFA at 4°C, cryoprotected in gradient 20% sucrose in PBS before being frozen by immersion in a cold isopentane bath (−60°C) for at least 5 min, and stored immediately at −80°C until sectioning. After serial sectioning, the sections were stained using the primary antibodies EP1536Y (Abcam) for detecting phospho S129–positive α-syn amyloid aggregates [dilution 1:5000 for immunohistochemistry (IHC) and 1:500 for immunofluorescence (IF)]. The slides were acquired using a Pannoramic slide scanner for IHC, and an Incucyte S3 High Content Imager (Sartorius) with a homemade 3D-printed slide holder for IF.

Electron microscopy

Aliquots of fibrillized samples were diluted with water, and one drop was applied to glow-discharged 300-mesh carbon-coated copper grids for 1 min. Grids were washed with one drop of water before being negatively stained with 2% uranyl acetate and dried for 5 min in the dark. Samples were observed using a Philips CM 120 (high-voltage 120 kV, lanthanum hexaboride filament) transmission electron microscope in low dose mode. Images were acquired using a Gatan US1000 (charge-coupled device) camera.

Solid-state NMR

All spectra were recorded on a Bruker NEO 800-MHz (^{1}H Larmor frequency) spectrometer with an ultrafast Bruker 0.7-mm HCND probe. The 0.7-mm rotor was placed into a 1.3-mm rotor with a rubber plug from the bottom. Approximately ~200 µl of fibrils resuspended in H_2O was pipetted in a funnel of filling tool, and it was spun for ~18 hours at 12°C at 29,500 rpm (with an SW32Ti Beckman ultracentrifugation rotor). The detailed NMR experimental parameters are described in tables S2 and S3.

SUPPLEMENTARY MATERIALS

Supplementary material for this article is available at http://advances.sciencemag.org/cgi/content/full/6/40/eabc4364/DC1

View/request a protocol for this paper from *Bio-protocol*.

REFERENCES AND NOTES

1. J. Burré, M. Sharma, T. C. Südhof, Cell biology and pathophysiology of α-synuclein. *Cold Spring Harb. Perspect. Med.* **8**, a024091 (2018).
2. J. Sun, L. Wang, H. Bao, S. Premi, U. Das, E. R. Chapman, S. Roy, Functional cooperation of α-synuclein and VAMP2 in synaptic vesicle recycling. *Proc. Natl. Acad. Sci. U.S.A.* **116**, 11113–11115 (2019).
3. B. Fauvet, M. K. Mbefo, M.-B. Fares, C. Desobry, S. Michael, M. T. Ardah, E. Tsika, P. Coune, M. Prudent, N. Lion, D. Eliezer, D. J. Moore, B. Schneider, P. Aebischer, O. M. El-Agnaf, E. Masliah, H. A. Lashuel, α-Synuclein in central nervous system and from erythrocytes, mammalian cells, and *Escherichia coli* exists predominantly as disordered monomer. *J. Biol. Chem.* **287**, 15345–15364 (2012).
4. U. Dettmer, A. J. Newman, F. Soldner, E. S. Luth, N. C. Kim, V. E. von Saucken, J. B. Sanderson, R. Jaenisch, T. Bartels, D. Selkoe, Parkinson-causing α-synuclein missense mutations shift native tetramers to monomers as a mechanism for disease initiation. *Nat. Commun.* **6**, 7314 (2015).
5. P. H. Weinreb, W. Zhen, A. W. Poon, K. A. Conway, P. T. Lansbury Jr., NACP, a protein implicated in Alzheimer's disease and learning, is natively unfolded. *Biochemistry* **35**, 13709–13715 (1996).
6. V. N. Uversky, J. Li, A. L. Fink, Evidence for a partially folded intermediate in α-synuclein fibril formation. *J. Biol. Chem.* **276**, 10737–10744 (2001).
7. M. G. Spillantini, R. A. Crowther, R. Jakes, M. Hasegawa, M. Goedert, α-Synuclein in filamentous inclusions of Lewy bodies from Parkinson's disease and dementia with Lewy bodies. *Proc. Natl. Acad. Sci. U.S.A.* **95**, 6469–6473 (1998).
8. P. Desplats, H.-J. Lee, E.-J. Bae, C. Patrick, E. Rockenstein, L. Crews, B. Spencer, E. Masliah, S.-J. Lee, Inclusion formation and neuronal cell death through neuron-to-neuron transmission of α-synuclein. *Proc. Natl. Acad. Sci. U.S.A.* **106**, 13010–13015 (2009).
9. K. C. Luk, C. Song, P. O'Brien, A. Stieber, J. R. Branch, K. R. Brunden, J. Q. Trojanowski, V. M.-Y. Lee, Exogenous α-synuclein fibrils seed the formation of Lewy body-like intracellular inclusions in cultured cells. *Proc. Natl. Acad. Sci. U.S.A.* **106**, 20051–20056 (2009).
10. H. Braak, K. D. Tredici, U. Rüb, R. A. I. de Vos, E. N. H. Jansen Steur, E. Braak, Staging of brain pathology related to sporadic Parkinson's disease. *Neurobiol. Aging* **24**, 197–211 (2003).
11. H. McCann, C. H. Stevens, H. Cartwright, G. M. Halliday, α-Synucleinopathy phenotypes. *Parkinsonism Relat. Disord.* **20**, S62–S67 (2014).
12. H. Heise, W. Hoyer, S. Becker, O. C. Andronesi, D. Riedel, M. Baldus, Molecular-level secondary structure, polymorphism, and dynamics of full-length α-synuclein fibrils studied by solid-state NMR. *Proc. Natl. Acad. Sci. U.S.A.* **102**, 15871–15876 (2005).

13. J. Gath, B. Habenstein, L. Bousset, R. Melki, B. H. Meier, A. Böckmann, Solid-state NMR sequential assignments of α-synuclein. *Biomol. NMR Assign.* **6**, 51–55 (2012).
14. J. Gath, L. Bousset, B. Habenstein, R. Melki, B. H. Meier, A. Böckmann, Yet another polymorph of α-synuclein: Solid-state sequential assignments. *Biomol. NMR Assign.* **8**, 395–404 (2014).
15. M. D. Tuttle, G. Comellas, A. J. Nieuwkoop, D. J. Covell, D. A. Berthold, K. D. Kloepper, J. M. Courtney, J. K. Kim, A. M. Barclay, A. Kendall, W. Wan, G. Stubbs, C. D. Schwieters, V. M. Y. Lee, J. M. George, C. M. Rienstra, Solid-state NMR structure of a pathogenic fibril of full-length human α-synuclein. *Nat. Struct. Mol. Biol.* **23**, 409–415 (2016).
16. J. Verasdonck, L. Bousset, J. Gath, R. Melki, A. Böckmann, B. H. Meier, Further exploration of the conformational space of α-synuclein fibrils: Solid-state NMR assignment of a high-pH polymorph. *Biomol. NMR Assign.* **10**, 5–12 (2016).
17. B. Li, P. Ge, K. A. Murray, P. Sheth, M. Zhang, G. Nair, M. R. Sawaya, W. S. Shin, D. R. Boyer, S. Ye, D. S. Eisenberg, Z. H. Zhou, L. Jiang, Cryo-EM of full-length α-synuclein reveals fibril polymorphs with a common structural kernel. *Nat. Commun.* **9**, 3609 (2018).
18. R. Guerrero-Ferreira, N. M. Taylor, A.-A. Arteni, P. Kumari, D. Mona, P. Ringler, M. Britschgi, M. E. Lauer, A. Makky, J. Verasdonck, R. Riek, R. Melki, B. H. Meier, A. Böckmann, L. Bousset, H. Stahlberg, Two new polymorphic structures of human full-length alpha-synuclein fibrils solved by cryo-electron microscopy. *eLife* **8**, e48907 (2019).
19. L. Bousset, L. Pieri, G. Ruiz-Arlandis, J. Gath, P. H. Jensen, B. Habenstein, K. Madiona, V. Olieric, A. Böckmann, B. H. Meier, R. Melki, Structural and functional characterization of two alpha-synuclein strains. *Nat. Commun.* **4**, 2575 (2013).
20. G. Bhak, J. Lee, T.-H. Kim, S. Lee, D. Lee, S. R. Paik, Molecular inscription of environmental information into protein suprastructures: Temperature effects on unit assembly of α-synuclein oligomers into polymorphic amyloid fibrils. *Biochem. J.* **464**, 259–269 (2014).
21. C. Kim, G. Lv, J. S. Lee, B. C. Jung, M. Masuda-Suzukake, C.-S. Hong, E. Valera, H.-J. Lee, S. R. Paik, M. Hasegawa, E. Masliah, D. Eliezer, S.-J. Lee, Exposure to bacterial endotoxin generates a distinct strain of α-synuclein fibril. *Sci. Rep.* **6**, 30891 (2016).
22. M.-R. Ma, Z.-W. Hu, Y.-F. Zhao, Y.-X. Chen, Y.-M. Li, Phosphorylation induces distinct alpha-synuclein strain formation. *Sci. Rep.* **6**, 37130 (2016).
23. W. Peelaerts, L. Bousset, A. Van der Perren, A. Moskalyuk, R. Pulizzi, M. Giugliano, C. Van den Haute, R. Melki, V. Baekelandt, α-Synuclein strains cause distinct synucleinopathies after local and systemic administration. *Nature* **522**, 340–344 (2015).
24. C. Peng, R. J. Gathagan, D. J. Covell, C. Medellin, A. Stieber, J. L. Robinson, B. Zhang, R. M. Pitkin, M. F. Olufemi, K. C. Luk, J. Q. Trojanowski, V. M.-Y. Lee, Cellular milieu imparts distinct pathological α-synuclein strains in α-synucleinopathies. *Nature* **557**, 558–563 (2018).
25. M. Shahnawaz, A. Mukherjee, S. Pritzkow, N. Mendez, P. Rabadia, X. Liu, B. Hu, A. Schmeichel, W. Singer, G. Wu, A.-L. Tsai, H. Shirani, K. P. R. Nilsson, P. A. Low, C. Soto, Discriminating α-synuclein strains in Parkinson's disease and multiple system atrophy. *Nature* **578**, 273–277 (2020).
26. A. Sidhu, J. Vaneyck, C. Blum, I. Segers-Nolten, V. Subramaniam, Polymorph-specific distribution of binding sites determines thioflavin-T fluorescence intensity in α-synuclein fibrils. *Amyloid* **25**, 189–196 (2018).
27. N. K. Polinski, L. A. Volpicelli-Daley, C. E. Sortwell, K. C. Luk, N. Cremades, L. M. Gottler, J. Froula, M. F. Duffy, V. M. Y. Lee, T. N. Martinez, K. D. Dave, Best practices for generating and using alpha-synuclein pre-formed fibrils to model Parkinson's disease in rodents. *J. Parkinsons Dis.* **8**, 303–322 (2018).
28. L. A. Volpicelli-Daley, K. C. Luk, T. P. Patel, S. A. Tanik, D. M. Riddle, A. Stieber, D. F. Meaney, J. Q. Trojanowski, V. M.-Y. Lee, Exogenous α-synuclein fibrils induce lewy body pathology leading to synaptic dysfunction and neuron death. *Neuron* **72**, 57–71 (2011).
29. L. A. Volpicelli-Daley, K. C. Luk, V. M.-Y. Lee, Addition of exogenous α-synuclein preformed fibrils to primary neuronal cultures to seed recruitment of endogenous α-synuclein to Lewy body and Lewy neurite–like aggregates. *Nat. Protoc.* **9**, 2135–2146 (2014).
30. A.-L. Mahul-Mellier, J. Burtscher, N. Maharjan, L. Weerens, M. Croisier, F. Kuttler, M. Leleu, G. Knott, H. A. Lashuel, The process of Lewy body formation, rather than simply alpha-synuclein fibrillization, is the major driver of neurodegeneration in synucleinopathies. biorXiv, 751891 [**Preprint**]. 2019. https://doi.org/10.1101/751891.
31. J. Zhang, A. Sandberg, A. Konsmo, X. Wu, S. Nyström, K. P. R. Nilsson, P. Konradsson, H. Le Vine III, M. Lindgren, P. Hammarström, Detection and imaging of Aβ1-42 and tau fibrils by redesigned fluorescent X-34 analogues. *Chemistry* **24**, 7210–7216 (2018).
32. F. Laferrière, Z. Maniecka, M. Pérez-Berlanga, M. Hruska-Plochan, L. Gilhespy, E.-M. Hock, U. Wagner, T. Afroz, P. J. Boersema, G. Barmettler, S. C. Foti, Y. T. Asi, A. M. Isaacs, A. Al-Amoudi, A. Lewis, H. Stahlberg, J. Ravits, F. De Giorgi, F. Ichas, E. Bezard, P. Picotti, T. Lashley, M. Polymenidou, TDP-43 extracted from frontotemporal lobar degeneration subject brains displays distinct aggregate assemblies and neurotoxic effects reflecting disease progression rates. *Nat. Neurosci.* **22**, 65–77 (2019).
33. G. Suzuki, S. Imura, M. Hosokawa, R. Katsumata, T. Nonaka, S.-I. Hisanaga, Y. Saeki, M. Hasegawa, α-Synuclein strains that cause distinct pathologies differentially inhibit proteasome. *eLife* **9**, e56825 (2020).
34. K. D. Volkova, V. B. Kovalska, A. O. Balanda, M. Y. Losytskyy, A. G. Golub, R. J. Vermeij, V. Subramaniam, O. I. Tolmachev, S. M. Yarmoluk, Specific fluorescent detection of fibrillar α-synuclein using mono- and trimethine cyanine dyes. *Bioorg. Med. Chem.* **16**, 1452–1459 (2008).
35. J. Cao, T. Wu, C. Hu, T. Liu, W. Sun, J. Fan, X. Peng, The nature of the different environmental sensitivity of symmetrical and unsymmetrical cyanine dyes: An experimental and theoretical study. *Phys. Chem. Chem. Phys.* **14**, 13702–13708 (2012).
36. A. A. Reinke, J. E. Gestwicki, Insight into amyloid structure using chemical probes. *Chem. Biol. Drug Des.* **77**, 399–411 (2011).
37. C. J. Sigurdson, K. P. R. Nilsson, S. Hornemann, G. Manco, M. Polymenidou, P. Schwarz, M. Leclerc, P. Hammarström, K. Wüthrich, A. Aguzzi, Prion strain discrimination using luminescent conjugated polymers. *Nat. Methods* **4**, 1023–1030 (2007).
38. E. T. Baker, J. W. Lavelle, The effect of particle size on the light attenuation coefficient of natural suspensions. *J. Geophys. Res.* **89**, 8197–8203 (1984).
39. J. Kaur, Application of UV Light Scattering to Detect Reversible Self-association and Aggregation of Proteins in Solution, *OpenCommons@UConn* (2017); https://opencommons.uconn.edu/dissertations/1386/.
40. K. C. Luk, V. Kehm, J. Carroll, B. Zhang, P. O'Brien, J. Q. Trojanowski, V. M.-Y. Lee, Pathological α-synuclein transmission initiates parkinson-like neurodegeneration in nontransgenic mice. *Science* **338**, 949–953 (2012).
41. T. Strohäker, B. C. Jung, S.-H. Liou, C. O. Fernandez, D. Riedel, S. Becker, G. M. Halliday, M. Bennati, W. S. Kim, S.-J. Lee, M. Zweckstetter, Structural heterogeneity of α-synuclein fibrils amplified from patient brain extracts. *Nat. Commun.* **10**, 5535 (2019).
42. M. Nishie, F. Mori, M. Yoshimoto, H. Takahashi, K. Wakabayashi, A quantitative investigation of neuronal cytoplasmic and intranuclear inclusions in the pontine and inferior olivary nuclei in multiple system atrophy. *Neuropathol. Appl. Neurobiol.* **30**, 546–554 (2004).
43. W.-L. Lin, M. W. DeLucia, D. W. Dickson, α-Synuclein immunoreactivity in neuronal nuclear inclusions and neurites in multiple system atrophy. *Neurosci. Lett.* **354**, 99–102 (2004).
44. N. J. Rutherford, A. N. Sacino, M. Brooks, C. Ceballos-Diaz, T. B. Ladd, J. K. Howard, T. E. Golde, B. I. Giasson, Studies of lipopolysaccharide effects on the induction of α-synuclein pathology by exogenous fibrils in transgenic mice. *Molecular Neurodegeneration.* **10**, 32 (2015).

Acknowledgments: We thank L. A. Largitte, L. Basurco, M. L. Thiolat, T. H. Nguyen, N. Biendon, and S. Dovero for technical help; T. Boraud and J.-P. Mazat for critical reading of the manuscript; and A. R. Crossman, Emeritus Professor, University of Manchester, UK, who read the revised the manuscript and made suggestions to improve readability. **Funding:** The project was conducted using financial support from the Region Nouvelle Aquitaine, the "Grand Prix" from the Del Duca Foundation, the European Research Council (ERC-2015-StG GA no. 639020), the Swiss National Science Foundation for early postdoc mobility project P2EZP2_184258, the CAMS Innovation Fund for Medical Sciences (CIFMS) grant (2016-I2M-2-006), the SAFEA: Introduction of Overseas Talents in Cultural and Educational Sector (G20190001626), the National Natural Science Foundation of China Grant (31970510), and the Innovative Medicines Initiative 2 Joint Undertaking under grant agreement no. 116060 (IMPRiND). This Joint Undertaking receives support from the European Union's Horizon 2020 research and innovation programme and EFPIA. This work is supported by the Swiss State Secretariat for Education, Research and Innovation (SERI) under contract number 17.00038. The opinions expressed and arguments used herein do not necessarily reflect the official views of these funding bodies. We thank the IR-RMN THC FR3050 CNRS and the Biophysical and Structural Chemistry platform (BPCS) at IECB for the access granted to their facilities. **Author contributions:** Conceptualization: F.D.G. and F.I. Validation and supervision: F.D.G., E.B., and F.I. Investigation and formal analysis: F.D.G., F.L., F.I., F.Z., A.Le., M.B., X.Y., E.M., A.G., E.D., B.H., N.D., J.D., S.C., and A.Lo. Methodology: F.D.G., F.I., F.L., B.H., E.F., C.Q., and A.Lo. Visualization: F.L., F.D.G., and F.I. Writing (original draft preparation): F.I. Writing (review and editing): F.D.G., F.L., E.B., B.H., A.Lo., and F.I. **Competing interests:** The authors declare that they have no competing interests. **Data and materials availability:** All data needed to evaluate the conclusions in the paper are present in the paper and/or the Supplementary Materials. Additional data related to this paper may be requested from the authors.

Submitted 24 April 2020
Accepted 11 August 2020
Published 2 October 2020
10.1126/sciadv.abc4364

Citation: F. De Giorgi, F. Laferrière, F. Zinghirino, E. Faggiani, A. Lends, M. Bertoni, X. Yu, A. Grélard, E. Morvan, B. Habenstein, N. Dutheil, E. Doudnikoff, J. Daniel, S. Claverol, C. Qin, A. Loquet, E. Bezard, F. Ichas, Novel self-replicating α-synuclein polymorphs that escape ThT monitoring can spontaneously emerge and acutely spread in neurons. *Sci. Adv.* **6**, eabc4364 (2020).

Science Advances

Novel self-replicating α-synuclein polymorphs that escape ThT monitoring can spontaneously emerge and acutely spread in neurons

Francesca De Giorgi, Florent Laferrière, Federica Zinghirino, Emilie Faggiani, Alons Lends, Mathilde Bertoni, Xuan Yu, Axelle Grélard, Estelle Morvan, Birgit Habenstein, Nathalie Dutheil, Evelyne Doudnikoff, Jonathan Daniel, Stéphane Claverol, Chuan Qin, Antoine Loquet, Erwan Bezard and François Ichas

Sci Adv **6** (40), eabc4364.
DOI: 10.1126/sciadv.abc4364